IEEE Access
Multidisciplinary | Rapid Review | Open Access Journal

SPECIAL SECTION ON COMPLEX NETWORKS ANALYSIS AND ENGINEERING IN 5G AND BEYOND TOWARDS 6G

Received May 28, 2020, accepted June 9, 2020, date of publication June 19, 2020, date of current version July 1, 2020.

Digital Object Identifier 10.1109/ACCESS.2020.3003734

Digital Twin for Metasurface Reflector Management in 6G Terahertz Communications

MANUS PENGNOO[1], MICHAEL TAYNNAN BARROS[2,4], LUNCHAKORN WUTTISITTIKULKIJ[1], BERNARD BUTLER[3], (Member, IEEE), ALAN DAVY[3], AND SASITHARAN BALASUBRAMANIAM[3], (Senior Member, IEEE)

[1]Department of Electrical Engineering, Faculty of Engineering, Chulalongkorn University, Bangkok 10330, Thailand
[2]CBIG at the BioMediTech, Faculty of Medicine and Health Technology, Tampere University, 33520 Tampere, Finland
[3]TSSG, Waterford Institute of Technology, X91 Y074 Waterford, Ireland
[4]School of Computer Science and Electronic Engineering, University of Essex, Colchester CO4 3SQ, U.K.

Corresponding authors: Manus Pengnoo (manus.pengnoo@gmail.com), Michael Taynnan Barros (m.barros@essex.ac.uk), and Sasitharan Balasubramaniam (sasib@tssg.org)

This work was supported by the Science Foundation Ireland via the Research Centre for Future Networks and Communications (CONNECT) under Grant 13/RC/2077.

ABSTRACT The performance demands from data-intensive applications, such as multimedia streaming, as well as the growing number of devices connecting to the Internet, will increase the need for higher capacity wireless communication links. The research community has recently explored regions of the spectrum, including the Terahertz band (0.1 THz to 10 THz), that are underutilised for communications. THz frequencies come with a plethora of special challenges, one of which is the very narrow effective beam, thereby requiring a Line of Sight (LoS) between sender and receiver. Researchers have explored the use of reflectors that can redirect beams around blockages. In this paper, we propose a THz signal guidance system where a Digital Twin is used to model, predict and control the signal propagation characteristics of an indoor space. Our approach finds the best THz signal path from the base station to the mobile target via the tunable metamaterial walls, avoiding obstacles as needed, using geometric (ray tracing), path loss and Terahertz Potential Field (THzPF) models. With this knowledge, the digital twin guides the selection of antenna strips at a base station and the reflectors along the signal path. A top-view camera, with advanced image processing, provides context updates (obstacle and mobile target locations) to the digital twin. The image processing system also senses factors like water vapour concentration, and the material composition and surface roughness of obstacles. Such factors affect propagation strength, and the digital twin modifies the beam paths to adapt. Simulation results have shown the efficiency of our control system to maintain a reliable signal connection while minimising the use of antenna and reflector strips. Our system is the first proposal that maximises THz signal-to-noise ratio (SNR) through such a dynamic and robust control system, which integrates image processing of a room with base station configuration.

INDEX TERMS Terahertz, digital twin, metasurface, 6G communications.

I. INTRODUCTION

Wireless communication systems have witnessed tremendous transformation through different generations over the years, where we have seen their scope expand beyond mobile devices, to machines and even wireless-enabled ''things''. The evolutionary steps from 1G to 5G have brought along dense heterogeneous networks that have opened new opportunities for new devices within the Internet of Things (IoT). They have also enabled new applications (e.g., autonomous vehicles, monitoring patients in a way that does not restrict their mobility and quality of life, or collecting data about the environment from distributed sensors). While this widespread connectivity has redefined how humans interact with each other and with machines, future wireless communications will require ever more capacity. This has triggered research regarding the next evolution of Beyond 5G and even 6G [1], [2]. As for the vision of developing the next generation wireless network system, 6G is expected to be available from 2030 [3]. There will be growth in various areas,

The associate editor coordinating the review of this manuscript and approving it for publication was Pedro Nardelli.

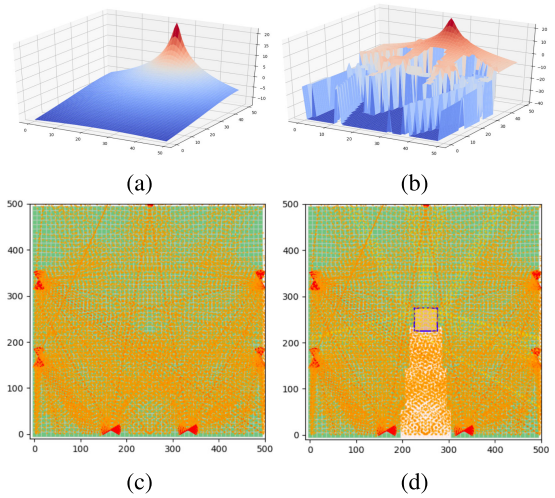

FIGURE 1. **Indoor THz signal strength scenarios for cases without (a), and with (b), obstacles. Ray tracing of signals with metasurface reflectors corresponding to cases (a) and (b) are shown in (c) and (d), respectively.**

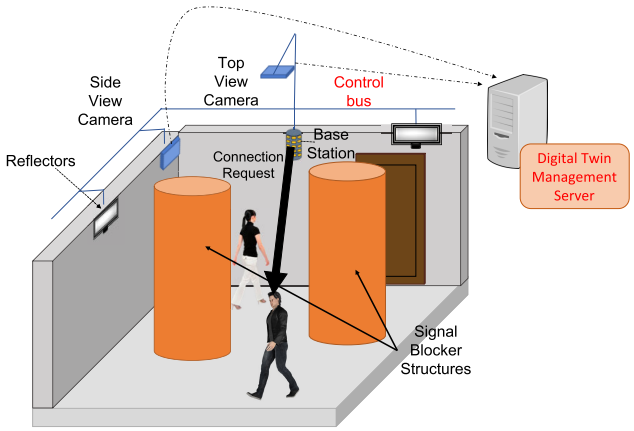

FIGURE 2. **Indoor architecture for Digital Twin management systems for THz communication system with metasurface reflectors, using image processing techniques to detect obstacles and construct a virtual *Terahertz Potential Field* (*THzPF*) to assist in directing the THz beams.**

including speed, number of supported devices, and the needs of supported applications will be very high compared to 5G. The 5G communications network has been developed and installed for service in many countries, with the main feature of the three main options being enhanced mobile broadband (eMBB), ultra-reliable low latency communications (URLLC), and massive machine-type communications (mMTC). In 6G communications, the key features are expected to be eMBB-Plus, secure ultra-reliable low-latency communications (SURLLC), three-dimensional integrated communications (3D-InteCom), unconventional data communications (UCDC), and big communications (BigCom) [4]. An important factor of the carrier spectrum is the demand for extremely large bandwidths [5], that promotes systems full efficiency, especially for indoor environments. Additional capacity is needed, not only to support new types of data-intensive services but also to enable new communication pathways between devices and machines [6], [7]. This vision of next-generation wireless communications is that ultra-high-speed data communications, reaching Terabits per second (Tbps) [8], will be needed. In order to target the data rate in the Terabit per second range, researchers are investigating new frequency spectra, ranging from *mm-wave* (60 GHz), sub-terahertz region, into the *Terahertz* (THz) band (0.3 - 10 THz) [9]. Since THz signals have such high frequency (equivalently, short wavelengths), each antenna strip can be scaled to a tiny size and built from metamaterials such as graphene [10]. However, numerous challenges apply to these high frequencies that are not traditionally found at lower frequencies used in previous generations of mobile wireless systems. Firstly, THz signals suffer significant signal attenuation in the form of energy loss due to free-space losses and atmospheric effects such as molecular absorption, so their range is more limited than equivalent signals in more commonly used frequency bands. As a possible solution, THz antennas take advantage of the shorter wavelengths of THz signals to narrow the THz beam, thereby maximising the range by maximising the desired energy of the signal along the required direction from source to target. This leads to the second major challenge, which is the requirement for an unobstructed Line-of-Sight (LoS) between the transmitter and the receiver. Thirdly, the extremely short wavelengths of THz signals means that they are scattered more easily by patterned surfaces, which appear "rough" in the THz band. Thus, instead of signals being reflected along the same path regardless of where they hit the surface, (i.e., specular reflection, as would happen with a "smooth" surface), they go in a variety of directions because of the local differences in the normal of the rough reflecting surface. Consequently, obstacles in the path tend to absorb THz signals (either directly or by non-specular reflection) rather than reflect the incoming signal in a way that enables this signal to be redirected to where it is required.

To address the problem of LoS-only propagation, the research community has proposed the use of intermediate reflectors, thereby enabling connectivity from source to target along a path made of a series of wireless links. For indoor settings, surfaces (walls and ceilings) can be constructed from metamaterials (we refer to them as metasurfaces) to help reflect and/or redirect beams. Such metasurfaces bounce signals between the base station and mobile endpoint, to avoid obstacles or environments that would otherwise attenuate or even block THz signals. Current research frontiers include programmable metamaterials for re-directing beams [11], [12] [13], mechanical control reflectors [14], [15] as well as protocols for security [16]. Fig. 1 illustrates how obstacles can block the THz signals and how reflective metasurfaces can help redirect the beams. Since THz signals require LoS to ensure adequate SNR, any adaptive beam steering control system needs to know the locations of obstacles that could block or lower the quality of THz signals. Using this information, it can predict the effect of those obstacles on the received signal strength and adjust

the signal paths to compensate for the presence of such obstacles.

In this paper, we propose a new management system for Metasurface Intelligent Environment for 6G, through the *Digital Twin* concept, which is illustrated in Fig. 2. Digital Twin is a virtual model of the physical indoor space, including objects within that space. Geometric analysis of beam propagation as well as energy models for beam reflection are central to a 6G Digital Twin that can measure both obstacles and user positions to analyse the channel information and improve overall performance through system adaptation. In this case, the Digital Twin models the THz signals and simulates any effects that can impact on the path loss. Our solution incorporates image processing techniques to capture any type of dynamic obstacles, such as a person in the room, to determine its profile. This object profile includes the size and dimensions of each obstacle as well as the texture of the material types that can affect the reflection or scattering properties of the THz signals. Image processing techniques can also capture the presence of some gases that can affect the THz signals through molecular absorption. By collecting this information, the Digital Twin will construct an SNR map with which to identify ideal virtual paths through a *Terahertz Potential Field* (*THzPF*), to provide accurate decisions on the best signal paths from the base station to the metasurface reflector that will redirect beams to the mobile endpoint [17]. The THzPF is inspired by the Artificial Potential Fields technique (APF) that is used for robotic real-time obstacle avoidance [18], [19]. The potential field is calculated based on attractive as well as repulsive forces to determine the best path around obstacles. We developed a ray-tracing simulator for the Digital Twin management system, where we focused on one particular type of programmable metasurface that is built from graphene gated structures to redirect beams using a voltage bias [10]. Our results show the benefits of the THzPF by analysing the overall SNR for varying numbers and material types of fixed obstacles, of users within the room, and several reflectors in fixed locations.

The rest of this paper is organised as follows: Section II presents the indoor THz communication system with the Obstacle detection system, Control system for the metasurface reflectors, and THzPF module. Section III presents the THzPF model, and this includes obstacle and texture detection, gradient calculation, while Section IV presents the simulation results. Lastly, Section V outlines the conclusions of this paper.

II. INDOOR THzPF MANAGEMENT SYSTEM

Our Digital Twin management system architecture is depicted in Fig. 3. The system is composed of three main components, which includes the *Controller*, *Base Station* and the *Metasurface reflector*. Two cameras (top and side view) feed images to the Controller server, which contains an online image processing module known as *You Only Look Once* (*YOLO*) machine learning algorithm [20]. This algorithm is used to detect the obstacles and identify the object's profile

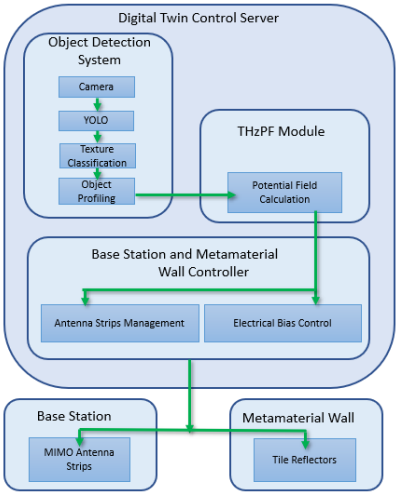

FIGURE 3. System diagram of the proposed THz signal guidance system. Based on a central controller server, it activates the antenna strips on the base station based on the THzPF created from the Obstacle Detection System and the Smart Reflector Module.

(its position and dimensions) using a monochromatic image of the obstacle. In addition to object detection, another Deep Learning algorithm is used for material type classification. The object profiles are passed on to the *THzPF* module, which determines the potential field based on SNR that models the scattering (diffraction) and reflection of signals that impinge on any obstacle. Based on the candidate beams with the highest THzPF value, the Controller determines the optimal path from the base station to the metasurface reflector and on to the mobile device (this is established through the *Potential Field Calculation* module). The path with the highest potential field determines the location on the metasurface reflector and the corresponding antenna strips that need to be turned on, which is managed by the *Antenna Strips Management* module. If beam steering is required at the reflector, an electrical bias is applied using the *Electrical Bias Control* module, and this sends control signals directly to the relevant reflector strips. In the following, we provide details that govern the basic theories involving the transmission and propagation of terahertz signals. Since we are interested only in the power distribution at the receiver, and not the extraction of the data signal from the beam that arrives at the receiver, we do not analyse the receiver model.

III. TERAHERTZ SYSTEMS AND PROPAGATION MODEL

This section presents background information on THz signals and their physical properties, particularly on factors that can affect the SNR.

A. TERAHERTZ BASE STATION MODEL

We consider a circular-section base station with a set I of antenna strips, where i represents an antenna strip ($i \in I$). All strips combine to form a 2D uniform array antenna with $M_I \times N_I = |I|$ total strips, where $M_a \times N_a$ is the total number

of active antenna elements placed vertically and horizontally, respectively, in the array. The *Antenna Strips Management* module of the Controller activates the antenna strips, thereby choosing the number of rays and their direction based purely on turning strips ON and OFF.

Array antennas can maximise the total link budget by increasing the antenna gain [21], [22], and in our case, they are needed to define a potential field that can be used to determine the most appropriate paths with the most reliable signals. By activating and deactivating particular antenna strips in different phases, active beam steering can be achieved. Directional beams are steered to the most appropriate location of the metasurface reflector to minimise NLoS transmission in the presence of blockages. To this end, we are interested in the calculation of the SNR at the receiver, but first, we need to calculate the base station gain (G_{bs}) based on the number of antenna strips and elements in each strip during the transmission period.

Given a number of antenna strips within the array, we consider the cone model approximations by Petrov *et al.* [9] for calculating the gain of the beam. For this, the power spectrum density of the signal p_{RX} at a distance r is represented as

$$p_{RX} = \frac{P_{Tx}}{S_A}, \tag{1}$$

where $S_A = 2\pi r^2$ is the surface area of the signal beam's spherical cap of radius r (whose axis is aligned with the propagation direction) and P_{Tx} is the transmitted signal power.

For signal cones that overlap with obstacles, the wavefront surface area will decrease by the obstacle loss percentage of ς. The resulting p_{RX}, based on the approximation from [9], is represented as

$$p_{RX} = \frac{P_{Tx}}{(2\pi rh\varsigma)} \tag{2}$$

where $h = r[1 - \cos(\alpha/2)]$ and α is the antenna directivity angle, and will also change for the case when obstacles block the signals, which is α'. We depict this information in Fig. 4.

Considering the signal free-space propagation model, we can calculate the antenna gain g_i for the main lobe in the antenna strip i of the cone model with a given α by considering $p_{RX} = P_{Tx}\frac{g_i}{(4r\pi r^2)}$, which is represented by

$$g_i = \frac{2}{1 - \cos(\alpha/2)}. \tag{3}$$

In our model, all antenna strips have the same gain values with the same directivity angle for every g_i, and the base-station antenna gain is relative to the total number of active elements based on the beam angle α. This angle determines the spread of rays in the cone and the active antenna elements that produced these rays. The total antenna gain from the base station is represented as follows

$$G_{bs} = \sum_{i=0}^{M_a \times N_a} g_i \tag{4}$$

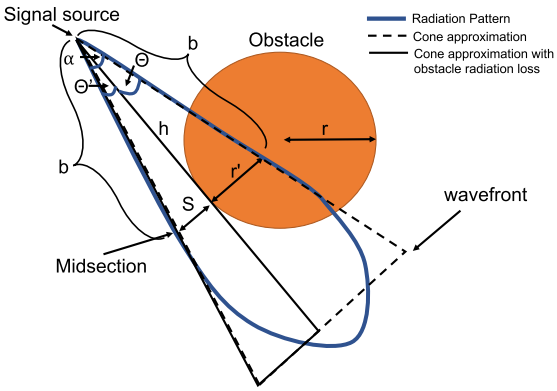

FIGURE 4. Diagram showing the parameters used in the calculation of the signal percentage loss (ς).

The base stations are assumed to have cylindrical geometry, with the axis in a vertical direction. Furthermore, we assume that the obstacles can also be approximated as cylinders with the same axis direction as the base stations. With this simplifying assumption, models are based on 2-D geometry and plane angles rather than 3-D geometry and robust angles.

Based on the free-space propagation model, the power spectral density (PSD) P_{Rx} for both use cases is represented as

$$P_{RX} = \begin{cases} P_{Tx} \cdot G_{bs}/(4\pi r^2), & \text{non-obstacle } (\varsigma = 1) \\ P_{Tx} \cdot G_{bs}/(4\pi r^2 \varsigma), & \text{obstacle.} \end{cases} \tag{5}$$

Signals within the beam area are dependent on the shape of the obstacle, and this will determine the transmitted portion of the beam (ς) in (5). We consider that the obstacle is in the midsection of the cone between the signal source and receiver, as illustrated in Fig. 4.

We produced an approximate model considering that 1) the triangle from the signal source to the midsection is an isosceles triangle with a top angle equal to the cone aperture angle (α) and 2) we broke the main triangle into two other isosceles triangles, a right triangle with top angle (θ) and a left triangle with top angle (θ'). We also consider that the total area of the midsection triangle is equal to the sum of the right and left triangles as well as that the difference between these triangles and the midsection triangle is the same as the whole cone triangle when it is divided with same top angles θ and θ'. Then, we can define

$$\varsigma = 100 \times \frac{A_{left}}{(A_{left} + A_{right})}. \tag{6}$$

Since α is a known value, we establish the relationship $\theta' = \theta - \alpha$. Thus the area of both triangles is

$$A_{left} = \frac{1}{2}b^2\sin(\theta'), \quad A_{right} = \frac{1}{2}b^2\sin(\theta). \tag{7}$$

The θ can be calculated by the following equation

$$\theta = \arcsin\left(\frac{r'}{b}\right). \tag{8}$$

In this paper we assume beams generate through phase-delay beamforming, since analog beamforming is reported adequate for for higher frequencies, such as for terahertz systems [23]. In addition, we avoid complex beamforming solutions, such as digital beamforming, and their respective increase in circuity design for beam generation [24].

B. TERAHERTZ PROPAGATION MODEL

In this section we describe the multi-ray propagation model for the $0.06 - 10$ THz band [14], [25], [26], which is considered in our study. The multi-ray model considers various factors that will affect the signal propagation, including: spreading ($\Psi(f,d)$), molecular absorption ($\beta(f,d)$), reflection ($\Gamma(f,d)$) and scattering ($\xi(f,d)$), in which f is the carrier frequency and d is the distance between the transmitter and receiver [27]. In the following, each of these effects is formulated.

1) SPREADING

Spreading in the THz-band is represented as follows,

$$\Psi(f,d) = \left(\frac{c}{4\pi f d}\right)^2, \tag{9}$$

where c is the speed of light in vacuum.

2) MOLECULAR ABSORPTION

The molecular absorption coefficient can be characterised as

$$k(f) = \sum_g \frac{p}{p_0}\frac{T_0}{T}\sigma^g(f), \tag{10}$$

where p is the standard pressure value in the room, p_0 is the reference pressure, T_0 is the standard temperature, T is the system temperature and $\sigma^g(f)$ is the absorption cross-section. Using the *Beer-Lambert* law that defines the transmittance of a high-frequency wave over an absorbing medium, we can represent the molecular absorption loss as

$$\beta(f,d) = e^{-\frac{1}{2}k(f)d}, \tag{11}$$

3) REFLECTION

The Kirchhoff theory is used for calculating the reflection loss of THz waves. The Fresnel reflection coefficient and the Rayleigh roughness factor are used for calculating the reflection loss, where the Fresnel reflection coefficient is represented as [28]

$$R(f) = \frac{cos(\theta_i) - n_t\sqrt{1-\left(\frac{1}{n_t}sin(\theta_i)\right)^2}}{cos(\theta_i) + n_t\sqrt{1-\left(\frac{1}{n_t}sin(\theta_i)\right)^2}} \tag{12}$$

where θ_i is the angle of the incident wave and n_t is the refractive index of a medium. The Rayleigh roughness factor is defined as

$$\rho(f) = e^{-\frac{G(f)}{2}}, \tag{13}$$

and

$$G(f) = \left(\frac{4\pi\omega cos(\theta_i)}{\lambda}\right)^2, \tag{14}$$

where ω is the standard deviation of the surface roughness and λ is the free space wavelength of the incident wave. Thus, the reflection loss can be represented as

$$\Gamma(f,d) = \sum_n \Psi(f,d)\cdot\beta(f,d)\cdot R(f)\cdot\rho(f), \tag{15}$$

in which n is the number of rays.

4) SCATTERING

Scattering affects THz signals based on the roughness level of the surface that it reflects. This is considered critical to the communication link and must also be taken into account. First, we consider the *Beckmann-Kirchhoff* theory for obtaining the scattering coefficient and its approximation [25], which is represented as:

$$\begin{aligned} S(f) = &-e^{\frac{-2cos(\theta_1)}{\sqrt{n_t{}^2-1}}} \\ &\cdot\sqrt{\frac{1}{1+g+\frac{g^2}{2}+\frac{g^3}{6}}} \\ &\cdot\sqrt{p_0^2+\frac{\pi cos(\theta_1)}{100}}ge^{v_s}+\frac{g^2}{4}e^{\frac{-vs}{2}}, \end{aligned} \tag{16}$$

in which, the values of p_0 is the renormalization constant, g is an approximation constant, v_s is a normalized coordinate coefficient and θ_1 is the zenith angle of the incident wave, and they can be found in [29]. Thus, the scattering loss can be obtained considering spreading, molecular absorption, the Rayleigh roughness factor and the scattering coefficient of n rays, and is represented as:

$$\xi(f,d) = \sum_n \Psi(f,d)\cdot\beta(f,d)\cdot R(f)\cdot S(f). \tag{17}$$

C. TERAHERTZ RECEIVER POWER MODEL

The path-loss model can be obtained upon adding the attenuation loss of each signal propagation effect (spreading (Ψ), molecular absorption (β), reflection (Γ) and scattering (ξ)) in dB, and this is represented as

$$\begin{aligned} \alpha(f,d) = &10\cdot\log_{10}(\Psi(f,d)) + 10\cdot\log_{10}(\beta(f,d)) \\ &+ 10\cdot\log_{10}(\Gamma(f,d)) + 10\cdot\log_{10}(\xi(f,r)). \end{aligned} \tag{18}$$

Based on this, the SNR is represented as

$$SNR(\alpha,d) = P_{tx} + G_{bs} + G_{rx} - \alpha(f,d) - \gamma - N, \tag{19}$$

where P_{tx} is the transmission power, G_{bs} is the antenna gain in the transmitter, and G_{rx} is the antenna gain in the receiver, N is the noise and γ is the loss resulting from shadowing. In order to simplify the SNR function for a specific scenario (which is also used for the rest of the paper), a simplified form was used from [30], which considers $P_{tx} = 1$ dBm with 7.4 dB conversion loss, G_{bs} and G_{rx} are equal to 30 dBi. In addition to this, we also consider that the receiver has a

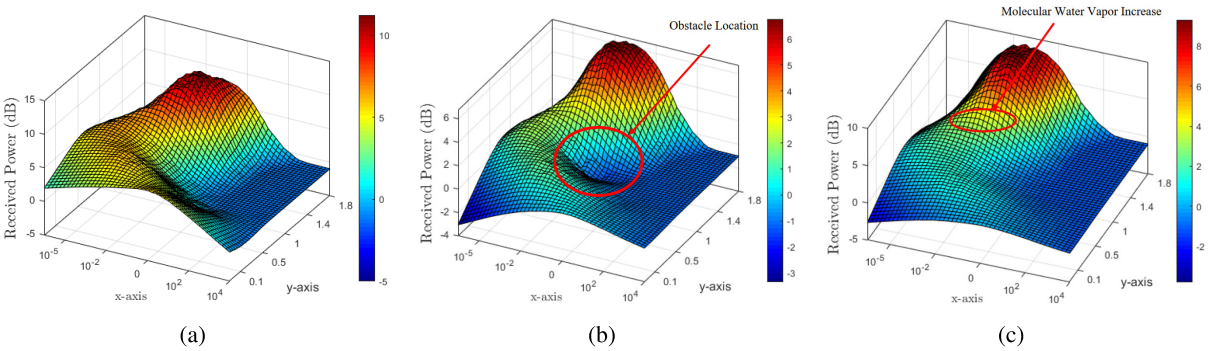

FIGURE 5. Different scenarios that impact the THz signal propagation that are reflected from the base station to the metasurface reflector (we assume no signal loss at the reflection point). (a) Shows the effects of distance, (b) shows the effects of blockage from a wood obstacle material, and (c) shows the effects of a micro humidity level increase (e.g. vapour from water spray).

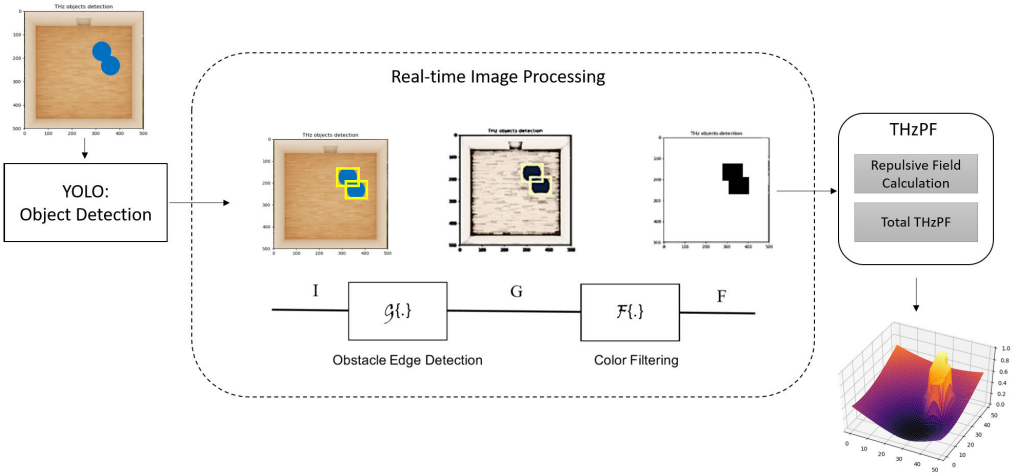

FIGURE 6. The process of repulse force vector creation from image processing and obstacle detection using the AI-based algorithm named YOLO (You-Only-Look-Once) for obtaining the repulsion gain (η). The obstacle edge detection is made later with a colour filtering for normalisation of the pixels. Finally, the total THzPF is calculated.

conversion gain of 8 dB with $N = 7.5$ dB and $\gamma = -74$ dBm, and this results in

$$SNR(\alpha, d) = 127.7 - \alpha(f, d). \quad (20)$$

However, we need to extend (20) to incorporate 1) the partial loss of signal strength due to absorption of an indoor obstacle, 2) the partial loss of signal strength from each reflection of the metasurface reflector. In our scenarios, we assume a group of signal reflections, and the new SNR for each signal is defined as

$$SNR(\alpha, d) = 127.7 - \alpha(f, d_1) \times \kappa_1 - \alpha(f, d_2) \times \kappa_2, \quad (21)$$

where d_1 is the distance between the base station and the metasurface reflector, d_2 is the distance between the wall and the receiver. The κ_1 and κ_2 are the probabilities of a signal irradiation pattern from the base station reaching the reflector and from the reflector reaching the receiver, respectively. The $S_r(f)$ is based on (16) but with additional effects of the signal reflection from the metasurface reflector. Since there are spaces between the reflector elements, the signal is not fully reflected, and the reflection index (n_t) in (12) needs to be adjusted accordingly. Fig. 5 shows the effects of the received reflected signal power when (a) there is no obstacle, (b) there is an obstacle in the centre of the room, and (c) when there is a molecular water vapour increase event in the room. Based on the simulation results in Fig. 5, considering the effects of various factors on THz signal levels, it is found that obstruction is the largest limitation that may result in insufficient signal coverage and caausing the user not being able to make a connection.

D. INTERFERENCE MODEL

In this section we propose an interference model from the partial reflection from an obstacle to a user equipment (UE). Fig. 7 shows the scenarios of partial reflection from an obstacle with a rectangular cross-section interfering a separate connection that is close enough to the obstacle that has either a flat surface (Fig. 7a) or a curved surface (Fig. 7b). We apply vector arithmetics to build an interference model that i) calculates the direction of the beam reflection from an obstacle

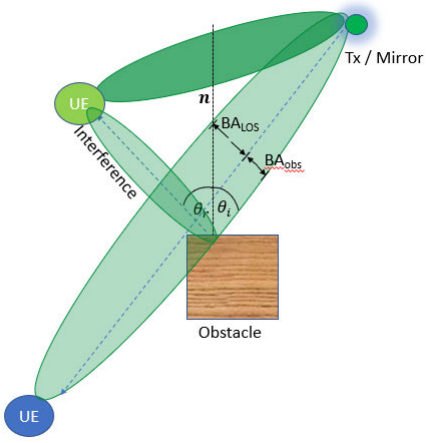

(a) Flat obstacle interference.

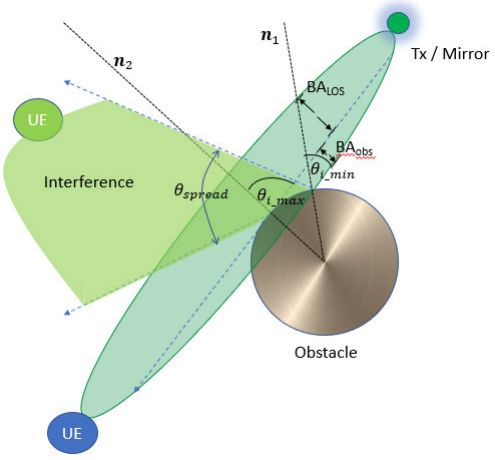

(b) Curved obstacle interference.

FIGURE 7. Top view geometric analysis on the partial interference caused from the partial reflection of the beam in a obstacle that is radiated from the Tx or reflector (mirror) to the blue user to the green user.

and ii) to calculates perpendicular, incident and reflection directions [31]. Considering the following equation:

$$\boldsymbol{BA_r} = \boldsymbol{BA_i} + 2\cos\theta_i \boldsymbol{n}, \tag{22}$$

where $\boldsymbol{BA_r}$ is the vector of reflected beam, $\boldsymbol{BA_i}$ is the vector of incident beam, θ_i is the incident angle, and $\boldsymbol{n}$ is the normal vector, orthogonal to the obstacle surface. The direction of the reflected beam can be calculated using the following equations

$$\cos\theta_i = -\boldsymbol{BA_i} \cdot \boldsymbol{n}, \tag{23}$$

thus,

$$\theta_r = \theta_i = -\cos^{-1}(\boldsymbol{BA_i} \cdot \boldsymbol{n}). \tag{24}$$

In the scenario of curved surface, the reflection of THz beam are depict in Fig. 7b. The partial beam reflection from a curved surface can be analyzed from the minimum incident angle ($\theta_{i_{\min}}$) to the maximum incident angle ($\theta_{i_{\max}}$). The reflected angles are varied as follows:

$$\theta_{\text{spread}} = |-\cos^{-1}(\boldsymbol{BA_i} \cdot \boldsymbol{n_2}) + \cos^{-1}(\boldsymbol{BA_i} \cdot \boldsymbol{n_1})|, \tag{25}$$

where θ_{spread} denoted size of reflected angle from a curved object. The directions of the interference range between $-\cos^{-1}(\boldsymbol{BA_i} \cdot \boldsymbol{n_2})$ and $-\cos^{-1}(\boldsymbol{BA_i} \cdot \boldsymbol{n_1})$. As shown in Fig 7b, the difference of reflections between a flat object and a curved object is the beam-spread angle of the reflected beam. The curved surface causes the reflected signal to spread in a wider angle, causing the signal strength to decrease as the angle increases. The proportion of signal strength caused by wide spread from reflection from a curved surface can be expressed as the equation below:

$$\rho = \frac{\alpha}{\theta_{\text{spread}}}, \tag{26}$$

where ρ is the beam angle ratio and α is the transmitted beam angle. We define the parameter Beam Ratio (BR_r) as the ratio of reflected beam area to the full beam area that can be calculated as the following equation:

$$BR_r = \frac{THzBA_{\text{obs}}}{THzBA_{\text{obs}} + THzBA_{\text{LOS}}}, \tag{27}$$

When considering each user, the aggregate interference, as described by [9], [32], from N sources reflections is defined as follows

$$I_{\text{agg}}(\boldsymbol{d}) = \sum_{i=1}^{N} P_{T_i} A d_i^{-2} e^{-Kd_i}, \tag{28}$$

with,

$$A = \frac{c^2}{16\pi^2 f^2}, \tag{29}$$

where $I_{\text{agg}}(\boldsymbol{d})$ is the aggregate interference, P_T is the transmitted power, $\boldsymbol{d}$ is the reflected beam displacement, d_i, $i = 1, 2, 3, \ldots N$. K is absorption coefficients, and A is spreading factor. With equal transmitted power for each beam, all P_{T_i} equal to P_{tx}, equation (28) and (29) can be rewritten as

$$I_{\text{agg}}(\boldsymbol{d}) = \left(NP_{tx}c^2(4\pi f)^{-2}\right) \cdot \sum_{i=1}^{N} d_i^{-2} e^{-Kd_i}, \tag{30}$$

When taking the beam ratio into consideration to find the interference power of each reflection, the aggregate interference can be represented as

$$I_{\text{agg}}(\boldsymbol{d}) = \left(NP_{tx}c^2(4\pi f)^{-2}\right) \cdot \sum_{i=1}^{N} d_i^{-2} e^{-Kd_i} \cdot BR_{r_i} \cdot \rho_i, \tag{31}$$

In the case of interference caused by reflections from a flat surface, ρ_i is set to 1. The signal-to-interference-plus-noise ratio for a user that is affected by interference of reflected beams can be characterized as:

$$\text{SINR}(\alpha, \boldsymbol{d}) = \frac{P_s(\alpha, d)}{P_n + I_{\text{agg}}(\boldsymbol{d}),} \tag{32}$$

where P_s is the received signal power at the UE, and P_n is the noise power. An example of heatmap simulation of signal

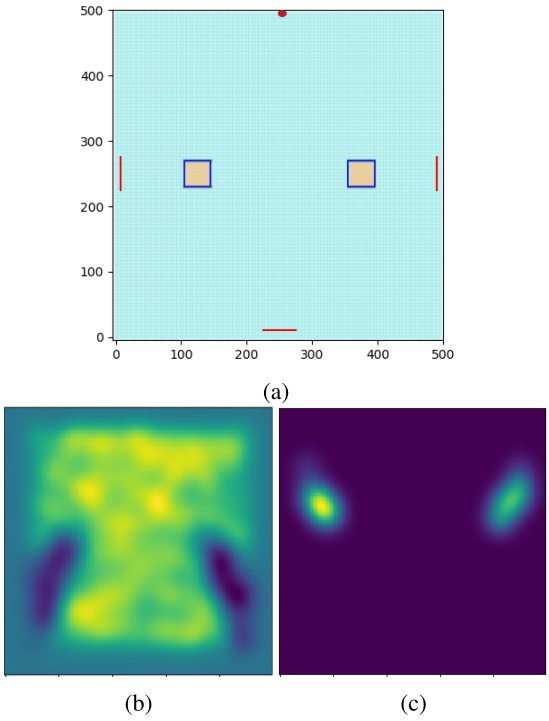

FIGURE 8. Statistical simulation of the signal power level received in a room with 2 smooth surface obstacles. (a) Statistical simulation of the signal power level received in a room with 2 smooth surface obstacles. (b) Heatmap of signal intensity calculated from motion simulation of user groups. (c) Heatmap only the reflection interference caused by the reflection of the beam area that hits the smooth surface obstacles.

levels and interference caused by reflections from smooth surfaces within an indoor environment can be illustrated as Fig. 8.

IV. TERAHERTZ POTENTIAL FIELD (THzPF)

The THzPF is a reactive model that defines a spatial gradient between two points (in our case a base station, and a metasurface reflector, as well as the receiver), and is obtained by differentiating a potential function THzPF : $\mathbf{R}^m \rightarrow \mathbf{R}$, where m is the number of spatial dimensions.

The potential function will have a continuous gradient when there are no obstacles, but in the event of any blockages or signal turbulence, this will be indicated through the rise in the potential field (or bumps that represent the obstacles). The potential function can be constructed with the sum of attractive $(\text{THzPF}(\text{SINR}(\alpha, d))_{Att,BA_i})$ and repulsive $(\text{THzPF}(\text{SINR}(\alpha, d))_{Rep,BA_i})$ potentials, which are described in the following subsections. Because of the way it is constructed, the THzPF is maximised near the transmitter and near any reflecting surface, and its spatial gradient is maximised in the direction of the THz rays that are emitted from either.

A. OBSTACLE AND TEXTURE DETECTION

An essential element in our THzPF gradient calculation is detecting and profiling the obstacles [33]. Even though sensors could be one solution, this can lead to high cost in placing the sensors in the environment, and in particular to get the right granularity in defining the profile of the object. As described earlier, our approach is based on image processing. Besides detecting the size of the obstacles using images, another benefit for characterising the impact of THz signals on the obstacles is materials and texture processing.

Based on recent advancement in object detection, we chose the **You-Only-Look-Once** (**YOLO**) method for proposing images to determine the obstacles. YOLO provides several advantages for our application, and this includes short processing time (25 milliseconds), real-time detection, multiple object detection. Our approach for the repulsive force calculation and its relationship with the total THzPF is shown in Fig. 6, where the obstacles detected by YOLO from an indoor image is converted into a repulsive force vector.

The steps for processing of images are as follows: First, the image is formatted, which typically means resizing the image. This is followed by obstacle detection using a convolutional neural network. Lastly, for the obstacle classification, a non-max suppression threshold-based algorithm is used to map the convolutional neural network output to simple rules. In this paper, we are only interested in the rules used for obstacle detection, where we consider the internal workings of YOLO as a black box.

To convert the YOLO output or the image with highlighted obstacles, we need to process the image further with a transformation mechanism. This method is illustrated in Fig. 6. First, we obtain the image with the obstacle edge detection (G) with $\mathbf{G} = \mathcal{G}\{\mathbf{I}\}$, then we obtain the monochromatic image $\mathbf{F}$ with all values between [0, 1] with the color filtering function $\mathbf{F} = \mathcal{F}\{\mathbf{G}\}$. Once the monochromatic image is created, the next step is to develop the virtual obstacle objects based on the dimensions of the image. These dimensions will be obtained from both the top as well as side-view cameras. Fig. 9 illustrates an example of the virtual obstacle object creation for two people that are in an indoor space.

Besides the obstacle detection and creation, the Digital Twin also incorporates a Deep Learning algorithm for material texture recognition. This is used to determine the reflective index n_t for the THz signals. Although scattering effects are not considered based on the material types, this can be incorporated in the future.

B. THzPF GRADIENT CALCULATION

The THzPF potential gradient ($\text{THzPF}_{\boldsymbol{BA_i}}$) is calculated for the selected beam area $\boldsymbol{BA_i}$. Fig. 10 presents an example of components within a beam area $\boldsymbol{BA_i}$ that consists of multiple signals with $\text{SINR}(\alpha, d)_{\boldsymbol{BA_i}}$. Effects (e.g., scattering, reflection) that occurs for each signal is virtually calculated in the $\text{SINR}(\alpha, d)_{\boldsymbol{BA_i}}$. The THzPF is relative to all the $\text{SINR}(\alpha, d)$ for each signal ray that can be transmitted as LOS directly from the base station, or from NLoS that is reflected from the metamaterial wall.

Between the source and the destination, there will be multiple paths with or not reflected signals. Depending on

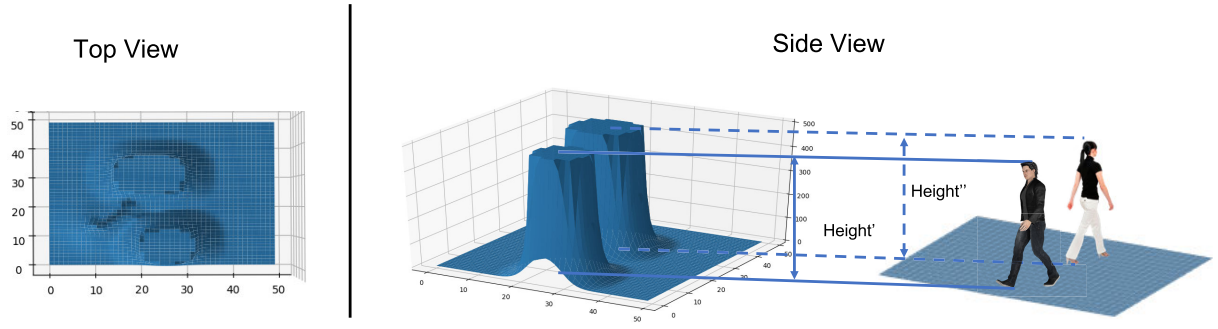

FIGURE 9. Illustration of obstacle object created after YOLO image processing for two people.

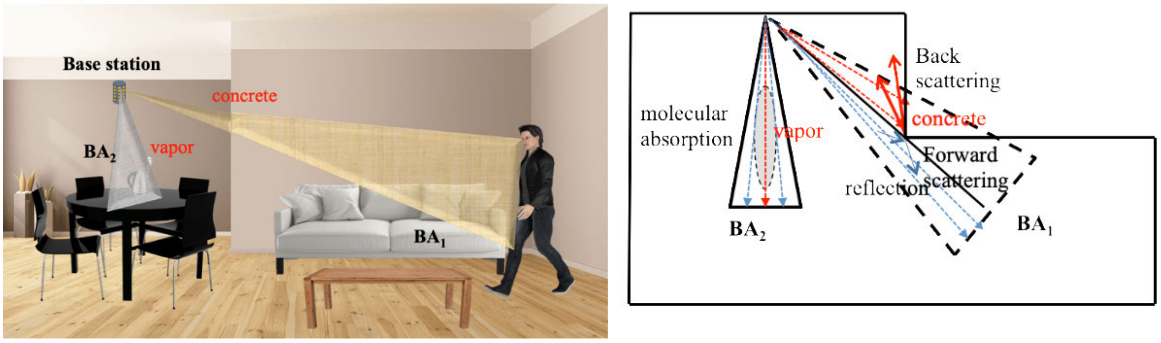

(a) (b)

FIGURE 10. Scenario of beam transmission in an indoor environment, (a) Illustration of Beam Area BA_i that is used in the potential field calculation, that incorporates all the effects that can affect the SNR_{BA_i}, (b) Top view diagram that shows various effects including the molecular absorption from water vapor, as well as the back scattering and forward scattering driven by the signal reflection on the wall in different reflection angles.

the configuration of blockage of a room, the different paths will have different SNR distribution per area, which is analogously considered as ''signal pressure''. These paths we term as *potential pressure paths*, by which is comprised of a flow area (FA) from the base station to the user. Effectively, the system will present j flow areas with multiple beams. We consider the characteristics as mentioned earlier to be able to define a new model for the THzPF gradient.

The THzPF gradient is represented as

$$\mathrm{THzPF}(\mathrm{SINR}_{\boldsymbol{BA_i},\boldsymbol{FAj}}(\alpha,d))_{FAj} = \left(\frac{\gamma}{(\Sigma\mathrm{SINR}_{\boldsymbol{BA_i},FAj}(\alpha,d)^2)}\right), \quad (33)$$

where γ represents the variance of SNR values inside a FA, and we define it as

$$\gamma = \frac{\Sigma(\mathrm{SINR}_{\boldsymbol{BA_i},FAj}(\alpha,d)^2) - \mathrm{E}[\mathrm{SINR}_{\boldsymbol{BA_i},\boldsymbol{FAj}}])}{|\mathrm{SINR}_{\boldsymbol{BA_i},\boldsymbol{FAj}}|}, \quad (34)$$

In this paper, we can consider the effect of signal interference when the base station sends beams to other users, by considering the reflection and scattering of static obstacles. Let $\boldsymbol{d_s}$ be the displacement of reflections from static obstacles which can be obtained by performing the vector operation:

$$\boldsymbol{d_s} = \boldsymbol{d} \cdot \boldsymbol{\delta}^T, \quad (35)$$

where $\boldsymbol{d}$ is the distance vector (displacement) and $\boldsymbol{\delta}$ is the vector of static-mobile presence indicator $\delta_i \in \{1, 0\}$. We model the analogous loss from interference in the THzPF gradient as well resulting in the equations expressed as follows, derived based on the condition that displacement of reflection is performed and, in that case, taking a quadratic inverse relationship with the SINR:

$$\mathrm{THzPF}_{\mathrm{Int}}(\mathrm{SINR}(\alpha,\boldsymbol{d_s})) = \begin{cases} (\dfrac{1}{\mathrm{SINR}(\alpha,\boldsymbol{d_s})})^2, & d \in \boldsymbol{d_s} > 0 \\ 0, & d \in \boldsymbol{d_s} = 0. \end{cases} \quad (36)$$

The total THzPF gradient for one FA is the sum of its THzPF gradient with its interference forces and is represented as:

$$\mathrm{THzPF}_{FA_i} = \mathrm{THzPF}_{FA_i}(\mathrm{SINR}_{\boldsymbol{BA_i},FAj}(\alpha,d)) + \mathrm{THzPF}_{\mathrm{Int}}(\mathrm{SINR}(\alpha,\boldsymbol{d_s})). \quad (37)$$

Fig. 11 presents an example of an optimal THzPF that is superimposed onto the obstacles. The example presents the lowest value of the THzPF, which is a path from the base station to the metasurface reflector (which may also include the beam steering process to get the ideal angle). Algorithm 1 presents the process for determining the $\mathrm{THzPF}_{\boldsymbol{BA_i}}$ based on

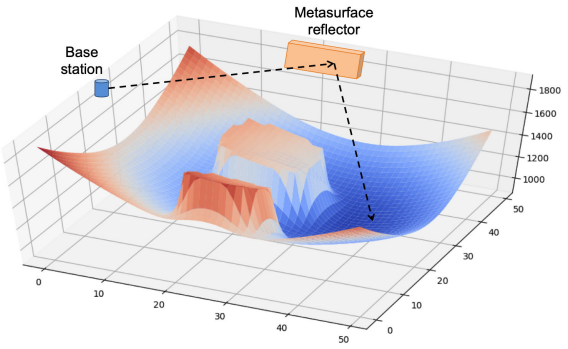

FIGURE 11. Example illustration of one optimum THzPF for a path that reflects from a metasurface.

the detected obstacles, as well as the optimum beam area $\boldsymbol{BA_i}$ that is selected. In some instances, beam steering is required at the metasurface reflectors to maximise the THz signals at the mobile device. Algorithm 2 presents the configuration of the beam steering mechanism in the reflector, where we will activate the relevant antenna elements on the base station for perfect alignment, as well as the electrical bias that is needed for steering the beam.

V. SIMULATIONS

This section will present the simulation scenario as well as the specific type of metamaterial wall used. The section will also present a performance analysis from the simulations.

A. SIMULATION SETUP

A THz ray-tracing simulator using Python has been developed to simulate the signals and analyse the propagation and reflection of THz signal paths.

In our scenario, the room is 5 × 5 meters, and this contains three obstacles with the size of 40 × 40 cm each. Our metamaterial wall width is set to 50 cm. The base station contains 40 antenna strips, where each is the size of 1 cm. The THz frequency considered is 0.3 THz.

Our simulation analysis considers two configurations, and this includes three and six metamaterial reflectors. The main features of the simulator include, (i) dimensioning of the indoor space and placements of objects by specifying their vertex position, (ii) placement of the base station transmitter, as well as position, size, and configurable angles of the metamaterial reflectors, (iii) simulating the rays that are emitted from the base station, as well as from the metamaterial reflectors, (iv) calculating the coverage areas and displaying this into multiple layers to analyse the details of interests, (v) generating THzPF from the information of base station location, mobile device location, obstacles, and metamaterial reflector locations, and (vi) calculating THz signal power in the interested area. For multiple mobile devices scenario, users will be random uniformly distributed to locations in the room with $X \sim U(0, room\_width)$ and $Y \sim U(0, room\_height)$.

Algorithm 1 Digital Twin-Based Cone Selection

Define: D is the Digital Twin of the indoor room, B is the set of blockages, $b \in B$, I_s is the side image of the room and I_t is the top image of the room. M is the set of metasurface mirrors, $m \in M$. T_x is the base station location, R_x is the mobile user location. $THzPF_{BA}$ is the potential field function with a beam area defined by the number of rays inside a cone. C set of possible cones from the base station, Z is the selected cone that is initially set to zero
function DigitalTwin(I_0) ▷ Image processing of the assisted by YOLO for Digital Twin Reconstruction
  $I_1 \leftarrow$ YOLO(I_t)
  for $i \leftarrow 1$ to $|I_1|$ **do**
    O $\leftarrow$ YOLO.Type(I_{1i}) ▷ Discover the type of object
    $b_i \leftarrow$ coordinate(x_1, y_1, x_2, y_2)
    b_i.height $\leftarrow$ b_i.getHeight(I_s)
    if O == 'Obstacle' **then**
      $B \leftarrow B$.append(b_i)
    end if
  end for
  $D \leftarrow B, M, T_x, R_x$
  return D
end function
function THZ_PF(D)
  $\text{THzPF}_{\text{BA}} \leftarrow 0$
  $\text{THzPF}_{\text{Total}} \leftarrow 0$
  $C_{\text{chosen}} \leftarrow 0$
  for $c \leftarrow 1$ to $|C|$ **do** ▷ Potential Field Calculation and Cone Selection
    if $|D.B| > 1$ **then**
      $\text{SINR}_c \leftarrow \sum \text{SINR}$ ▷ Eq. (21)
    else
      $\text{SINR}_c \leftarrow \sum \text{SINR}$ ▷ Eq. (20)
    end if
    $\text{THzPF} \leftarrow \text{THzPF}_{\text{BA}_c}(\text{SINR}_c)$ ▷ Eq. 37
    if THzPF.BA > $\text{THzPF}_{\text{total}}.BA$ **then**
      $\text{THzPF}_{\text{total}} \leftarrow$ THzPF
      $C_{\text{chosen}} \leftarrow$ c
    end if
  end for
  return $\text{THzPF}_{\text{Total}}$
end function
$I_s \leftarrow$ `SideCamera.get()` ▷ Side Image Acquisition Process
$I_t \leftarrow$ `TopCamera.get()` ▷ Top Image Acquisition Process
$D \leftarrow$ `DigitalTwin`(I_s, I_t) ▷ Digital Twin Reconstruction
Cone $\leftarrow$ `THZ_PF(D)` ▷ Cone Selection

B. GRAPHENE-ENABLED TUNABLE METAMATERIAL WALL

There have been many works in recent times that have developed non-absorbing or non-scattering metasurface walls for

Algorithm 2 Smart Beam Steering Using THzPF

Define: M is the set of metasurface mirrors, $m \in M$. T_x is the transmitter, R_x is the interested receiver. THzPF is the field function of THzPF including the attractive field ($\text{THzPF}_{\text{Att}}$) and the repulsive field ($\text{THzPF}_{\text{Rep}}$). The potential field gradient THzPF_{BA} is the potential of interested beam area (BA)

function bias(m, R_X)
  `bias` ← False
  `bias_angle` ← 0
  if θ_{normal} <> θ_{R_x} **then**
    `bias` ← True
    $d_\theta \leftarrow \theta_{\text{normal}} - \theta_{R_x}$
    `bias_angle` ← d_θ
  end if
  return `bias, bias_angle`
end function
`bias_list` ← null
`THzPF` ← `THZ_PF(B, M, T_x, R_x, α)`
for $R_X \in All\_UE$ **do**
  if `NLOS(T_x,R_x,THzPF)` **then**
    for $m \in M$ **do**
      `bias,bias_angle` ← `BIAS(m,R_X)`
      `bias_list.append(bias,bias_angle)`
    end for
    `max_snr` ← 0
    for $i \in$ `All_BA(bias_list,beamAreas)` **do**
      if SINR(THzPF_{BA_i}) > `max_snr` **then**
        `max_snr` ← SINR(THzPF_{BA_i})
      end if
    end for
    steering_{R_x} ← `max_snr`
  end if
end for

reflecting electromagnetic waves [34], and an in particular programmable metasurfaces [11], [35].

In this paper, we focus on graphene-based metasurface reflectors [10], which can achieve dynamic switching of THz beam reflection through tunable metasurfaces that can be electronically controlled. By applying a Fermi-energy E_F to produce a current bias that activates a specific group of reflector elements inside an array, THz beams can be redirected from the base station towards the receiver that has an incident angle of the range 2π to $\pi/4$.

The metasurface wall illustrated in Fig. 12 is composed of an array of graphene-based tiles (reflector elements) with heterogeneous geometry characteristics. The reflector resonant frequency will change as well as a shift in the dispersion curve based on the geometry as well as the arrangement of the tiles. To control the bias electronically, the different sized tiles require a double graphene layer gate structure that contains a

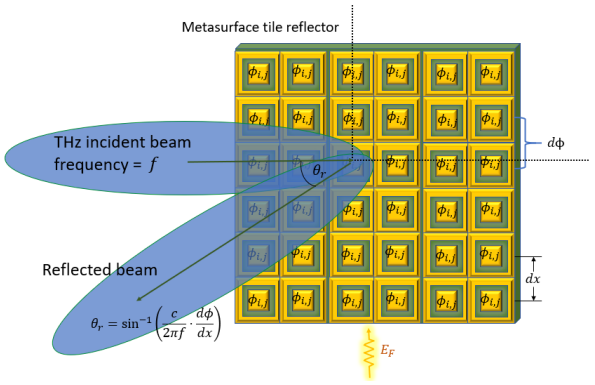

FIGURE 12. Structure of the metasurface graphene reflector. Each reflector element is uniformly distributed over the metasurface area. Upon reception of DC voltage with energy value E_F, each element array will be activated. Beam steering will occur when the beam is aligned to a specific group of reflector elements that produce the angle of steering.

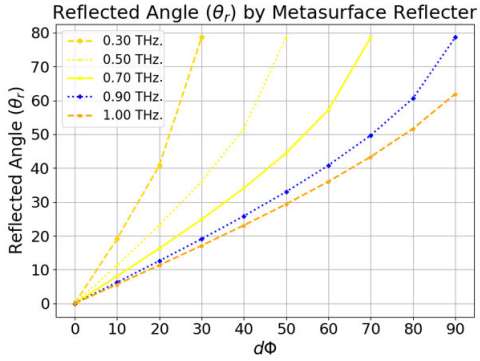

FIGURE 13. Different THz beam steering angle controlled by the $d\Phi$ variation with a fixed dx at 85 μm.

thin silicon dioxide insulating film. This insulating file will operate as a reflection amplitude modulator.

1) VARYING THz SIGNAL REFLECTION

The variation in the reflection angleθ_r based on the incidence angle θ_i of a beam is based on the Snell's law and is represented as follows

$$\sin(\theta_r) = \sin(\theta_i) = \frac{\lambda_0}{2\pi n_i}\frac{d\Phi}{dx}, \tag{38}$$

where λ_0 is the wavelength in free space, n_i is the refractive index of the metasurface material, and $d\Phi/dx$ represents the phase gradient on distance dx. Fig. 13 presents the relationship between the beam steering angle of the incident beam by varying the $d\Phi/dx$, which is increased from 0 to 80 degrees when the phase slope is increased from 0 to 40 degrees. The range of reflected angle that can range from 0 to 2π will depend on the arrangement of size tiles that can be arranged across the width of the reflector.

2) GRAPHENE METASURFACE TILE ENERGY COST BIAS

The bias that is applied to a tile reflector element is through a DC bias voltage. This is achieved by applying a Fermi Energy

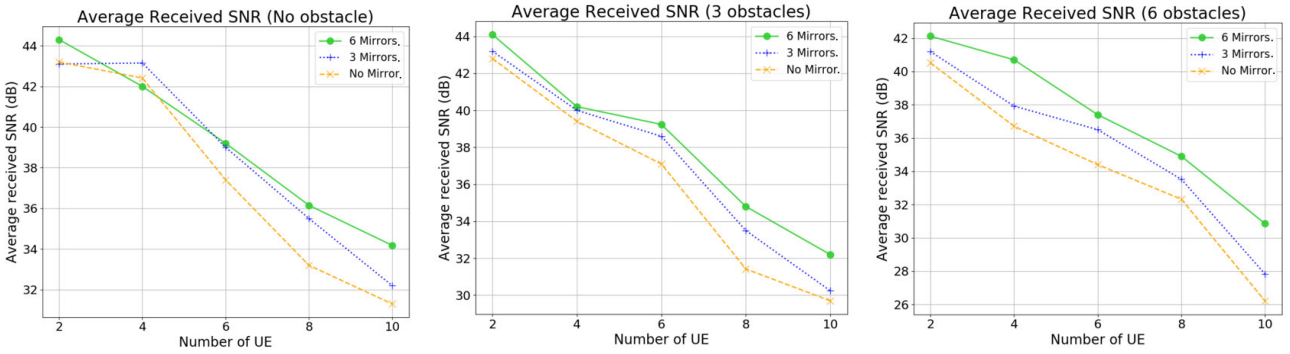

FIGURE 14. The number of obstacles, reflectors and users impact on the system's SNR. (a) no obstacle (b) 3 obstacles and (c) 6 obstacles.

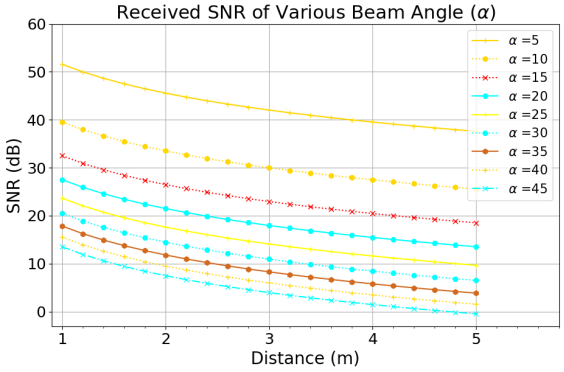

FIGURE 15. SNR results with variation of the beam angle (α).

E_F level for each element, which controls the conductivity of the sandwiched graphene as well as an insulating film. The Fermi Energy level bias on the reflector and its relationship to the bias voltage V_g is represented as [10]

$$E_F \approx \hbar v_f \sqrt{\frac{\pi \epsilon_r \epsilon_0 V_g}{e t_s}}, \tag{39}$$

where ϵ_r and ϵ_0 are the permittivity of the thin-film insulating layer between the gated graphene elements and vacuum, respectively, and e and v_f are the electron charge and the Fermi velocity (1.1×10^6 m/s in graphene), respectively. Depending on the angle that is to be reflected from the metasurface, the cost for the beam steering ξ will be $E_F \times N_e$, where N_e is the number of reflector elements required to achieve the reflected angle θ_r. In this paper, for simplicity of energy cost calculations, we consider that E_F are equal for all reflector elements in the metasurface.

C. IMPACT ON SYSTEM's SNR WITH RESPECT TO NUMBER OF OBSTACLES AND METASURFACE REFLECTORS

The main objective of the proposed virtual THz signal guidance system is to maximise the signal beams at the receiver. We initially evaluate the SNR of an indoor environment, and how it gets impacted by the number of obstacles, metasurface reflectors as well as users. We consider three configurations for the metasurface reflectors, and this includes no reflector, three reflectors, six reflectors with three different sets of scenarios: (a) no obstacle (b) three obstacles and (c) six obstacles. The results of this experiment are presented in Fig. 14. For all scenarios, as the number of user increases, the average SNR starts to decrease due to the increasing number of beams with a high potential field that is reflected from the metasurface, which leads to longer beam propagation distances as opposed to straight LoS rays, as depicted in Fig. 14 (a), (b) and (c). This decrease can reach up to 18 dB with ten users. With an increase in the number of obstacles ((b) with three obstacles and (c) with six obstacles), the benefit from the number of metasurface reflectors becomes clearer, with a maximum gain of 5 dB when using six reflectors. This gain becomes obvious as the number of users increases because there is a higher number of potential fields between the base station and the user through the tunable metasurface reflectors.

In addition, from the analysis of the signal level, we can adjust the system design to have the signal level that is suitable for use by adjusting the beam angle as shown in Fig. 15. The simulation result in Fig. 15 shows the SNR resulting from the adjustment of the beam angle between 5 degrees to 45 degrees. A narrower beam can provide a higher SNR, but will also have a smaller beam area and a greater chance of being blocked by obstacles.

D. EVALUATION OF THE THzPF BEAM STEERING SIGNAL GUIDANCE

We aim to quantify what are the costs in providing beam steering from the metasurface reflectors based on the THzPF virtual signal guidance for multiple users. Fig. 16 shows the beam propagation based on the image processing for object detection, as well as the quantity of Fermi energy to enable signal reflection for users that are blocked. As part of this simulation, we also include the materials texture classification based on Deep Learning, and this classification is shown in Fig. 17. We have four different scenarios, including (a)

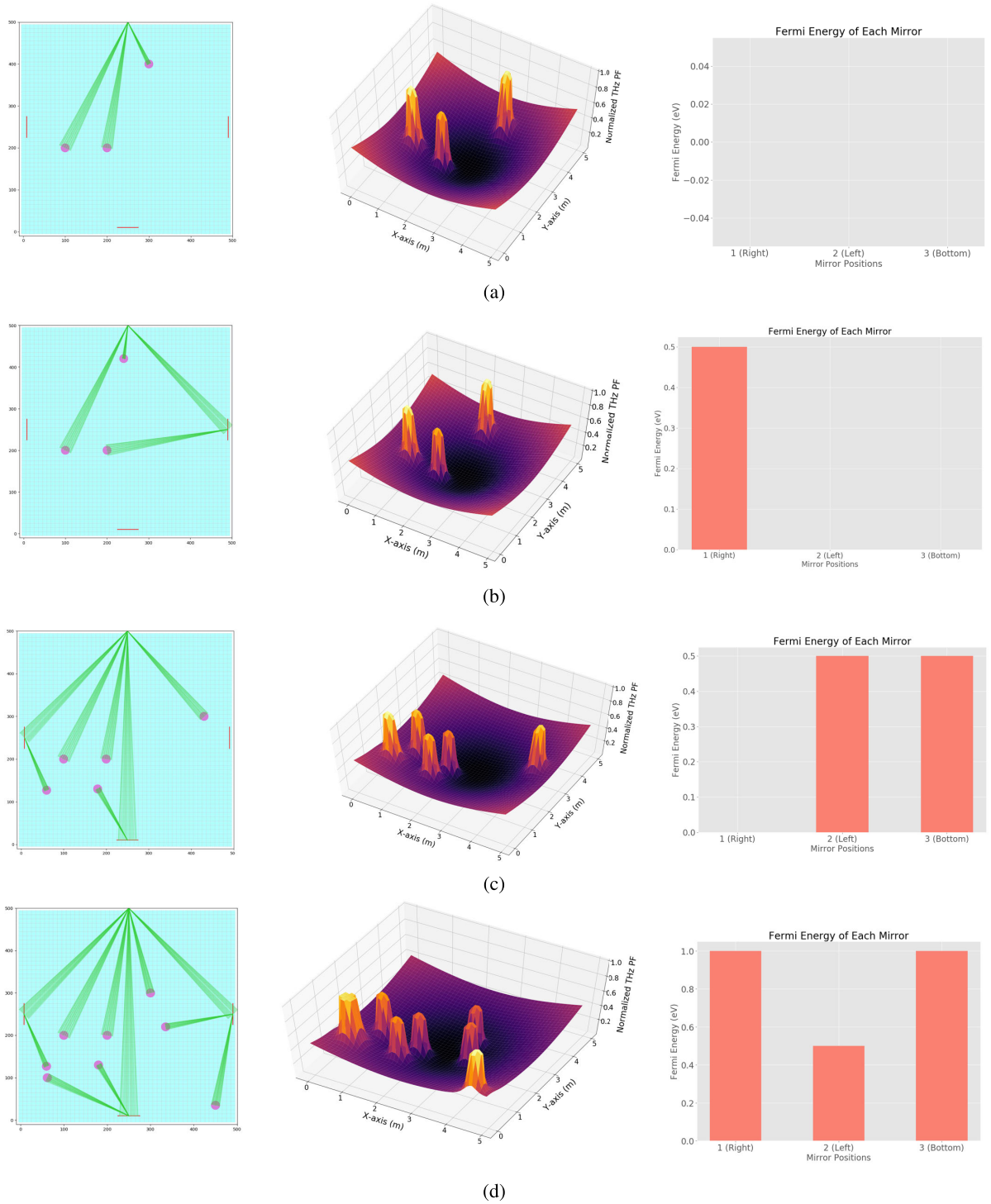

FIGURE 16. Beam distribution from the transmitter to users both LoS and NLoS (left), THzPF of the real-time system (center), and Fermi energy level of each reflector (right). Scenarios are (a) 3 users with all LoS. In this case all users have LoS from the transmitter, the signal will be transmitted directly from the transmitter to each user., (b) 3 users with 1 beam steering, (c) 5 users with 2 beam steering, (d) 8 users with 5 beam steering. In (b) - (c) the system calculates the best possible signal path that can reflect the signal from one of the metasurface reflectors to blocked users. The metasurface mirror will bias the elements that give each aligned beam at a Fermi energy of 0.5 eV.

three users with all LoS, (b) three users with one beam steering event (c) five users with two beam steering events, and (d) eight users with five beam steering events. The simulation is set to have a transmitter and three metasurface reflectors on each side of the wall. The object detection system detects the location of users walking at various locations and calculates

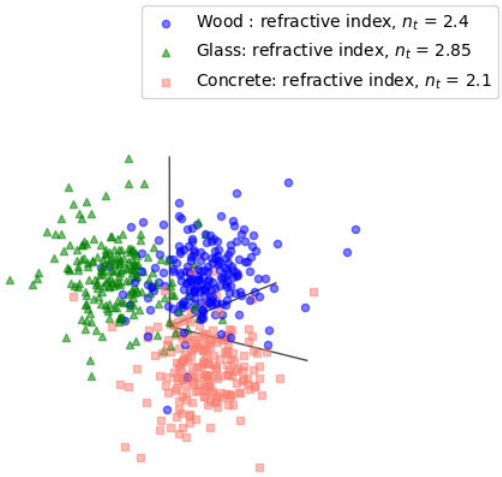

FIGURE 17. Classification of different wood, glass, and concrete reflective index using Deep Learning algorithm for materials and texture analysis.

the THzPF to analyse the beam path based on Algorithm 2. In the case that all users have LoS from the transmitter, the signal will be transmitted directly from the transmitter to each user as shown in Fig 16 (a), and will not require any electronic bias at the metasurface reflectors. Fig 16 (b) shows that the system can detect the movement of three users, and in particular when one mobile device is blocked by another user. The system calculates the best possible signal path that can reflect the signal from one of the metasurface reflectors to the blocked user. The result is that the signal is sent to the right mirror, and the metasurface mirror will bias the elements that give the aligned beam at a Fermi energy of 0.5 electron Volt (eV) according to Algorithm 2. In Fig 16 (c) and (d) the number of users is 5 and 8, respectively. The number of steered beams were two and five, respectively. The results show that the use of metasurface-reflector can help users in high-speed wireless communication systems that need LoS signals to avoid obstacles, including the human body. The amount of electric bias also shows the amount of users who have been connected to the signals that the control system can manage through Digital Twin management system.

The subsequent analysis is the calculation of the energy costs of the reflected as well as steered beams with a varying number of obstacles and users. The different simulation cases for this scenario include, 1) without metasurface reflectors 2) three metasurface reflectors, and 3) six metasurface reflectors. Fig. 18 shows the results of the electric bias Fermi energy (E_F) for different number of obstacles. From the simulation results, we can see that as the number of users increases the biasing effect for reflecting and steering the beam costs also increase. Considering the increase in the number of reflectors, the cost of electrical bias is also increased, which means more users can be helped by reflectors and we should design the installation of reflectors in an appropriate number in order to cope with obstacles in various cases.

We also show the superiority of the presented THzPF with the analysis of the variation of the number of users from

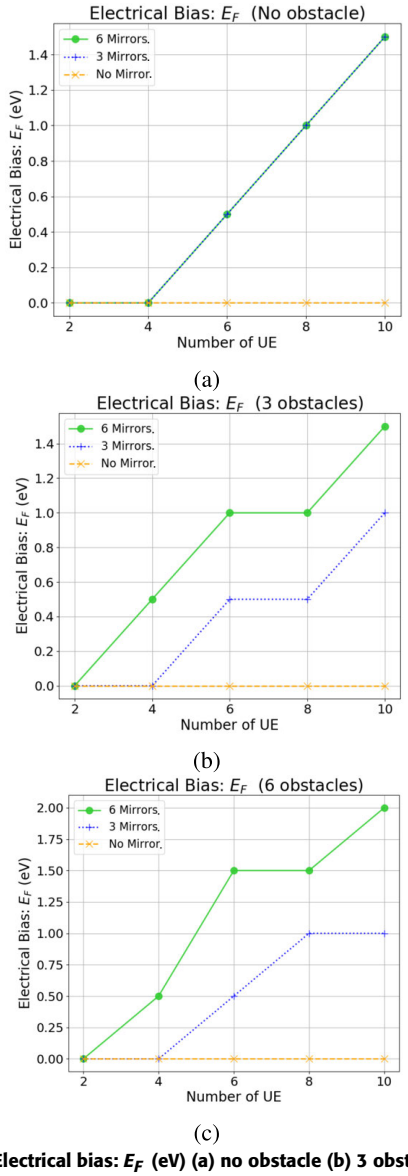

FIGURE 18. Electrical bias: E_F (eV) (a) no obstacle (b) 3 obstacles and (c) 6 obstacles.

zero to 30 effects in the average received power as well as the cumulative E_F for all number of users. The results are depicted in Fig. 19. The average received power maintains instable while using the THzPF while increasing the number of users, Fig. 19 a). Besides that, there is an average gain of approximately 10 dB power when not using the THzPF. There is a considerable variation of the received power with the number of users, due to their random location allocation in our simulations. Using the THzPF, this variation decreases to very small variations, which indicates the efficiency in system-wide adaptation to user location, starting from the YOLO prediction of user location till overcoming blockages and reflecting appropriate signals with the THzPF. Even though there is no mobility models in the simulations of users, we expect that THzPF might also provide benefits in that regard, which should be investigated as future work. There is the energy cost associated with the THzPF user increase

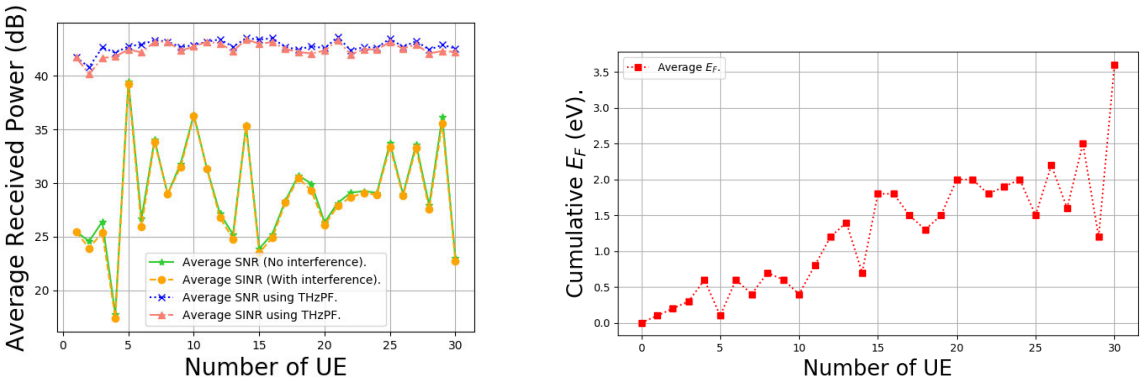

FIGURE 19. The result of the mean value of the received signal power, which consists of the effect of reflection with different number of users. (a) The result of the mean value of the received signal power, which consists of the effect of reflection. (b) The average bias energy used by the THzPF calculation to operate metasurface mirrors.

adaptation, as we show in Fig. 19 b). The costs will vary with user location, so the number of reflections needed to maintain stable, received power will also vary. However, it is clear that the continuous linear increase in cumulative E_F with the increase in the number of users. Based on the simulation analysis, the ability to know the position of the users and obstacles to knowing the virtual beams that are most suitable for the user is a clear advantage.

VI. CONCLUSION

Now that THz frequencies are receiving attention for future high-speed wireless links, the research community is trying to solve the propagation limitations of this newly explored spectrum band. Blockages from obstacles cause the base station to mobile endpoint connections to fail because the obstacles induce coverage blackspots for direct beams to and from the THz base stations. A proposed approach that has gained attention recently is the use of metasurface reflectors that can reflect and steer THz beams around such obstacles.

In this paper, we propose a signal guidance and control system that uses a Digital Twin of the space where THz signal propagation is to be optimised. The Digital Twin is used to derive candidate signal paths that ensure transmission even in the presence of obstacles, where reflectors are present to change the direction of the THz beams as needed. The resulting Controller includes modules to perform complex calculations, including ray tracing, path loss prediction, and antenna, reflector and mobile endpoint alignment. The underlying signal model is a bundle of rays characterised by a new signal propagation metric called Terahertz Potential Fields (THzPF). The Controller ensures that the antenna strip selected for emitting the signal has a line of sight from the base station to the mobile endpoint, if necessary via a reflector and that the available signal paths maximise the SNR of the local THzPF field. Since knowledge of the obstacles' size, position and movement are essential for calculating the THzPF, a set of cameras stream images of the space and these images are processed in a way that ensures the Digital Twin is synchronised with the actual disposition of the space. Indeed the processed images can be used by the Controller to refine the transmission model and the THzPF so that it takes account of the material composition and surface roughness of obstacles. This information can be overlaid on the larger scale existing propagation model, to predict the effects of forward and backscatter of the THz signals on the THzPF.

Simulation results have shown the effectiveness of using the THzPF to guide THz signals to reach the mobile endpoint, while also ensuring that only a small number of antenna strips need to be activated, thus minimising energy consumption. Our proposed solution is the first step towards an autonomous THz propagation control system to provide and maintain reliable high-capacity connections for users in spaces. Indeed, unlike traditional base stations, our proposed THz propagation control system features sensing (by a Controller assigned to one or more THz base stations) of the space served by a given THz base station and uses both physical models and machine learning to maintain reliable, high-bandwidth THz links with the mobile endpoints the base station serves. The mobile endpoints themselves do not require such ambient intelligence. Each UE will receive functioning information from the base station that already performs the intelligence. The UE will then know where and where transmissions are reflected and to which mirror they must focus on. This is a perfectly reasonable idea, where many protocols for 5G, and even before that, use geospatial information sharing between the base station and the UE [36], [37].

Future research will consider both micro and macro-mobility of users, and how metasurface reflector handovers can be performed to ensure uninterrupted connectivity. The micro-mobility will consider small physiological movements (e.g., moving arms holding the mobile endpoints) that might make the mobile endpoint loose connectivity. The future work will also consider different architectures of the metasurface reflectors, which may include such devices being placed on, or even embedded in, the wall as well as the ceilings to assist in more efficient steering of the beams.

REFERENCES

[1] I. F. Akyildiz, S. Nie, S.-C. Lin, and M. Chandrasekaran, "5G roadmap: 10 key enabling technologies," *Comput. Netw.*, vol. 106, pp. 17–48, Sep. 2016.

[2] I. Akyildiz, J. Jornet, and C. Han, "TeraNets: Ultra-broadband communication networks in the terahertz band," *IEEE Wireless Commun.*, vol. 21, no. 4, pp. 130–135, Aug. 2014.

[3] M. Latva-Aho and K. Leppänen, "Key drivers and research challenges for 6G ubiquitous wireless intelligence," Univ. Oulu, Oulu, Finland, White Paper, 2019. [Online]. Available: http://jultika.oulu.fi/files/isbn9789526223544.pdf

[4] S. Dang, O. Amin, B. Shihada, and M.-S. Alouini, "What should 6G be?" *Nature Electron.*, vol. 3, no. 1, pp. 20–29, Jan. 2020.

[5] M. H. Alsharif, A. H. Kelechi, M. A. Albreem, S. A. Chaudhry, M. S. Zia, and S. Kim, "Sixth generation (6G) wireless networks: Vision, research activities, challenges and potential solutions," *Symmetry*, vol. 12, no. 4, p. 676, Apr. 2020.

[6] C. Bockelmann, N. Pratas, H. Nikopour, K. Au, T. Svensson, C. Stefanovic, P. Popovski, and A. Dekorsy, "Massive machine-type communications in 5G: Physical and MAC-layer solutions," *IEEE Commun. Mag.*, vol. 54, no. 9, pp. 59–65, Sep. 2016.

[7] M. M. Butt, E. A. Jorswieck, and N. Marchetti, "On optimizing power allocation for reliable communication over fading channels with uninformed transmitter," *IEEE Trans. Wireless Commun.*, vol. 17, no. 10, pp. 6617–6629, Oct. 2018.

[8] C. Liaskos, S. Nie, A. Tsioliaridou, A. Pitsillides, S. Ioannidis, and I. Akyildiz, "A new wireless communication paradigm through software-controlled metasurfaces," *IEEE Commun. Mag.*, vol. 56, no. 9, pp. 162–169, Sep. 2018.

[9] V. Petrov, M. Komarov, D. Moltchanov, J. M. Jornet, and Y. Koucheryavy, "Interference and SINR in millimeter wave and terahertz communication systems with blocking and directional antennas," *IEEE Trans. Wireless Commun.*, vol. 16, no. 3, pp. 1791–1808, Mar. 2017.

[10] Y. Zhang, Y. Feng, J. Zhao, T. Jiang, and B. Zhu, "Terahertz beam switching by electrical control of graphene-enabled tunable metasurface," *Sci. Rep.*, vol. 7, no. 1, Dec. 2017, Art. no. 14147.

[11] C. Liaskos, A. Tsioliaridou, A. Pitsillides, S. Ioannidis, and I. Akyildiz, "Using any surface to realize a new paradigm for wireless communications," *Commun. ACM*, vol. 61, no. 11, pp. 30–33, Oct. 2018.

[12] C. Liaskos, S. Nie, A. Tsioliaridou, A. Pitsillides, S. Ioannidis, and I. Akyildiz, "Realizing wireless communication through software-defined HyperSurface environments," in *Proc. IEEE 19th Int. Symp. World Wireless, Mobile Multimedia Netw. (WoWMoM)*, Jun. 2018, pp. 14–15.

[13] S. Nie, J. M. Jornet, and I. F. Akyildiz, "Intelligent environments based on ultra-massive MIMO platforms for wireless communication in millimeter wave and terahertz bands," in *Proc. IEEE Int. Conf. Acoust., Speech Signal Process. (ICASSP)*, May 2019, pp. 7849–7853.

[14] M. T. Barros, R. Mullins, and S. Balasubramaniam, "Integrated terahertz communication with reflectors for 5G small-cell networks," *IEEE Trans. Veh. Technol.*, vol. 66, no. 7, pp. 5647–5657, Jul. 2017.

[15] C. Jansen, R. Piesiewicz, D. Mittleman, T. Kurner, and M. Koch, "The impact of reflections from stratified building materials on the wave propagation in future indoor terahertz communication systems," *IEEE Trans. Antennas Propag.*, vol. 56, no. 5, pp. 1413–1419, May 2008.

[16] X. Yu, D. Xu, Y. Sun, D. W. K. Ng, and R. Schober, "Robust and secure wireless communications via intelligent reflecting surfaces," 2019, *arXiv:1912.01497*. [Online]. Available: http://arxiv.org/abs/1912.01497

[17] M. Pengnoo, M. T. Barros, L. Wuttisittikulkij, W. Asdornwised, A. Davy, and S. Balasubramaniam, "Overcoming blockage with artificial potential field assisted mirror reflectors for terahertz communications," in *Proc. 3rd Int. Balkan Conf. Commun. Netw. (BalkanCom)*, 2019.

[18] T. W. Dunbar and J. M. Esposito, "Artificial potential field controllers for robust communications in a network of swarm robots," in *Proc. 32th Southeastern Symp. Syst. Theory (SSST)*, 2005, pp. 401–405.

[19] P. Vadakkepat, K. C. Tan, and W. Ming-Liang, "Evolutionary artificial potential fields and their application in real time robot path planning," in *Proc. Congr. Evol. Comput. (CEC)*, vol. 1, 2000, pp. 256–263.

[20] R. Zhang, Y. Yang, W. Wang, L. Zeng, J. Chen, and S. McGrath, "An algorithm for obstacle detection based on YOLO and light filed camera," in *Proc. 12th Int. Conf. Sens. Technol. (ICST)*, Dec. 2018, pp. 223–226.

[21] T. Merkle, A. Tessmann, M. Kuri, S. Wagner, A. Leuther, S. Rey, M. Zink, H.-P. Stulz, M. Riessle, I. Kallfass, and T. Kurner, "Testbed for phased array communications from 275 to 325 GHz," in *Proc. IEEE Compound Semiconductor Integr. Circuit Symp. (CSICS)*, Oct. 2017, pp. 1–4.

[22] C. Lin and G. Y. Li, "Indoor terahertz communications: How many antenna arrays are needed?" *IEEE Trans. Wireless Commun.*, vol. 14, no. 6, pp. 3097–3107, Jun. 2015.

[23] C. Lin and G. Y. Li, "Adaptive beamforming with resource allocation for distance-aware multi-user indoor terahertz communications," *IEEE Trans. Commun.*, vol. 63, no. 8, pp. 2985–2995, Aug. 2015.

[24] P.-Y. Chen, C. Argyropoulos, and A. Alù, "Terahertz antenna phase shifters using integrally-gated graphene transmission-lines," *IEEE Trans. Antennas Propag.*, vol. 61, no. 4, pp. 1528–1537, Apr. 2013.

[25] C. Han, A. O. Bicen, and I. F. Akyildiz, "Multi-ray channel modeling and wideband characterization for wireless communications in the terahertz band," *IEEE Trans. Wireless Commun.*, vol. 14, no. 5, pp. 2402–2412, May 2015.

[26] S. Priebe and T. Kurner, "Stochastic modeling of THz indoor radio channels," *IEEE Trans. Wireless Commun.*, vol. 12, no. 9, pp. 4445–4455, Sep. 2013.

[27] J. M. Jornet and I. F. Akyildiz, "Channel modeling and capacity analysis for electromagnetic wireless nanonetworks in the terahertz band," *IEEE Trans. Wireless Commun.*, vol. 10, no. 10, pp. 3211–3221, Oct. 2011.

[28] J. Kokkoniemi, J. Lehtomäki, and M. Juntti, "Reflection coefficients for common indoor materials in the terahertz band," in *Proc. 5th ACM Int. Conf. Nanosc. Comput. Commun.*, Sep. 2018, p. 22.

[29] J. E. Harvey, "Modified Beckmann–Kirchhoff scattering model for rough surfaces with large incident and scattering angles," *Opt. Eng.*, vol. 46, no. 7, Jul. 2007, Art. no. 078002.

[30] C. Jansen, S. Priebe, C. Moller, M. Jacob, H. Dierke, M. Koch, and T. Kurner, "Diffuse scattering from rough surfaces in THz communication channels," *IEEE Trans. THz Sci. Technol.*, vol. 1, no. 2, pp. 462–472, Nov. 2011.

[31] B. D. Greve. (2006). *Reflections and Refractions in Ray Tracing*. [Online]. Available: http://www.flipcode.com/archives/reflection_transmission.pdf

[32] R. Zhang, K. Yang, Q. H. Abbasi, K. A. Qaraqe, and A. Alomainy, "Analytical characterisation of the terahertz *in-vivo* nano-network in the presence of interference based on TS-OOK communication scheme," *IEEE Access*, vol. 5, pp. 10172–10181, 2017.

[33] L. Khamsawad, M. Pengnoo, P. Sasithong, P. Vanichchanunt, L. Wuttisittikulkij, M. T. Barros, and S. Balasubramaniam, "Simulation of signal coverage for terahertz communications," in *Proc. 33rd Int. Tech. Conf. Circuits/Syst., Comput. Commun. (ITC-CSCC)*, 2018, pp. 1–4.

[34] S. Ju, S. H. A. Shah, M. A. Javed, J. Li, G. Palteru, J. Robin, Y. Xing, O. Kanhere, and T. S. Rappaport, "Scattering mechanisms and modeling for terahertz wireless communications," in *Proc. IEEE Int. Conf. Commun. (ICC)*, May 2019, pp. 1–7.

[35] A. C. Tasolamprou *et al.*, "Exploration of intercell wireless millimeter-wave communication in the landscape of intelligent metasurfaces," *IEEE Access*, vol. 7, pp. 122931–122948, 2019.

[36] M. Z. Shafiq, L. Ji, A. X. Liu, J. Pang, and J. Wang, "Geospatial and temporal dynamics of application usage in cellular data networks," *IEEE Trans. Mobile Comput.*, vol. 14, no. 7, pp. 1369–1381, Jul. 2015.

[37] S. Kaasalainen, L. Ruotsalainen, M. Kirkko-Jaakkola, O. Nevalainen, and T. Hakala, "Towards multispectral, multi-sensor indoor positioning and target identification," *Electron. Lett.*, vol. 53, no. 15, pp. 1008–1011, Jul. 2017.

MANUS PENGNOO received the B.Eng. degree in electrical engineering from Srinakarinwirot University, Bangkok, Thailand, in 2002, the M.Eng. degree in telecommunication engineering from the King Mongkut's Institute of Technology Ladkrabang, Thailand, in 2008, and the M.B.A. degree in aviation management from Chulalongkorn University, Bangkok, in 2011, where he is currently pursuing the Ph.D. degree in electrical engineering.

From 2005 to 2014, he was a Project Manager and a Senior Engineer with major telecommunication companies, Thailand. From 2015 to 2016, he was an Assistant to Commissioner and a Researcher with the National Broadcasting and Telecommunications Commission (NBTC), Thailand. His research interests include satellite communications, cognitive radio, artificial intelligence in communications, intelligent systems in biomedical science, and terahertz science for 6G communications.

MICHAEL TAYNNAN BARROS received the B.Tech. degree in telematics from the Federal Institute of Education, Science and Technology, in 2011, the M.Sc. degree in computer science from the Federal University of Campina Grande, in 2012, and the Ph.D. degree in telecommunication software from the Waterford Institute of Technology, in 2016.

He is currently a Lecturer with the School of Computer Science and Electronic Engineering, University of Essex, U.K. He has authored or coauthored over 60 research articles in various international flagship journals and conferences in the areas of wireless communications, molecular and nanoscale communications, and bio nanoscience. He has participated the Technical Program Committee. His research interests include the Internet of Bio Nanothings, molecular communications, bio nanoscience, and 6G Communications. He is a recipient of the Marie Skłodowska Curie Individual Fellowship (MSCA-IF), BioMediTech Institute, Tampere University, Finland. He also serves as a Reviewer for many journals and various international conferences.

LUNCHAKORN WUTTISITTIKULKIJ received the B.Eng. degree in electrical engineering from Chulalongkorn University, Bangkok, Thailand, in 1990, and the M.Sc. and Ph.D. degrees in telecommunications from the University of Essex, U.K., in 1992 and 1997, respectively.

In 1995, he was involved with the European Commission Funded Project, such as Multiwavelength Transport Network (MWTN) responsible for network design and dimensioning. In 1997, he joined the Faculty of Engineering, Chulalongkorn University, where he is currently an Associate Professor with the Department of Electrical Engineering. He is the author of 13 books and over 50 research articles. His research interest includes broadband wireless access networks.

BERNARD BUTLER (Member, IEEE) received the B.Sc. degree in applied maths and computing, the M.Sc. degree in applied maths from University College Cork, Ireland, and the M.Sc. degree in communication software and the Ph.D. degree from the Waterford Institute of Technology (WIT), Ireland.

He was a Senior Research Scientist with the Scientific Software Section, National Physical Laboratory, U.K., working on mathematical and statistical support for metrology (measurement science). He was a Business Intelligence and Data Mining Consultant working with major companies in the telecommunications, banking, insurance, retail, and medical devices sectors, Ireland. He was a Visiting Researcher in data centre performance with Amadeus, France. He is currently a Senior Research Fellow and a Manager with the Emerging Networks Laboratory, Telecommunications Software and Systems Group, Waterford Institute of Technology. His research interests include scalable access control, management of distributed computing systems, high-precision networking, system performance and machine learning, and applied to smart cities and data center operations.

ALAN DAVY received the B.Sc. degree (Hons.) in applied computing and the Ph.D. degree from the Waterford Institute of Technology, Waterford, Ireland, in 2002 and 2008, respectively.

He has been with TSSG (student), since 2002. He was a Postdoctoral Researcher, in 2008. In 2010, he was with IIT Madras, India, as an Assistant Professor in network management systems. He returned to the TSSG and appointed as a Senior Research Fellow, where he was a Research Unit Manager with the Emerging Networks Laboratory, in 2014. In 2019, he was the Head of the Department of Computing and Mathematics, Waterford Institute of Technology. He received the Marie Curie International Mobility Fellowship, in 2010, which brought him to work with the Universitat Politècnica de Catalunya, for a period of two years.

SASITHARAN BALASUBRAMANIAM (Senior Member, IEEE) received the B.E. degree in electrical and electronic engineering from The University of Queensland, Brisbane, QLD, Australia, in 1998, the M.E. degree in computer and communication engineering from the Queensland University of Technology, Brisbane, in 1999, and the Ph.D. degree from The University of Queensland, in 2005.

He is currently the Director of the Research with the Telecommunication Software and Systems Group, Waterford Institute of Technology, Waterford, Ireland. He is a Principal Investigator with the Science Foundation Ireland and the VistaMilk (SFI) Research Centre. He is also a Funded Investigator with the SFI CONNECT and the FutureNeuro Research Centres. He has authored or coauthored more than 100 articles in various journals and conferences and actively participates in a number of technical program committees for various conferences. His current research interests include molecular communications, the Internet of (Bio) NanoThings, and terahertz wireless communications.

Dr. Balasubramaniam is on the Steering Board Committee of ACM NANOCOM, which he Co-Founded. In 2018, he was the IEEE Nanotechnology Council Distinguished Lecturer. He has served as an Associate Editor for the IEEE Internet of Things Journal. He serves as an Associate Editor for the IEEE Transactions on Molecular, Biological and Multi-Scale Communications, the IEEE Letters of the Computer Society, *Nano Communication Networks* (Elsevier), and *Digital Communication and Networks* (Elsevier).